Article

Europium-Diethylenetriaminepentaacetic Acid (Eu-DTPA) Loaded Radioluminescence Liposome Nano-Platform for Effective Radioisotope-Mediated Photodynamic Therapy

Wooseung Lee, Miyeon Jeon, Jinyeong Choi, Chiwoo Oh, Gaeun Kim, Seongmoon Jung, Changsoon Kim, Sung-Joon Ye, and Hyung-Jun Im

ACS Nano, **Just Accepted Manuscript** • DOI: 10.1021/acsnano.0c04324 • Publication Date (Web): 21 Aug 2020

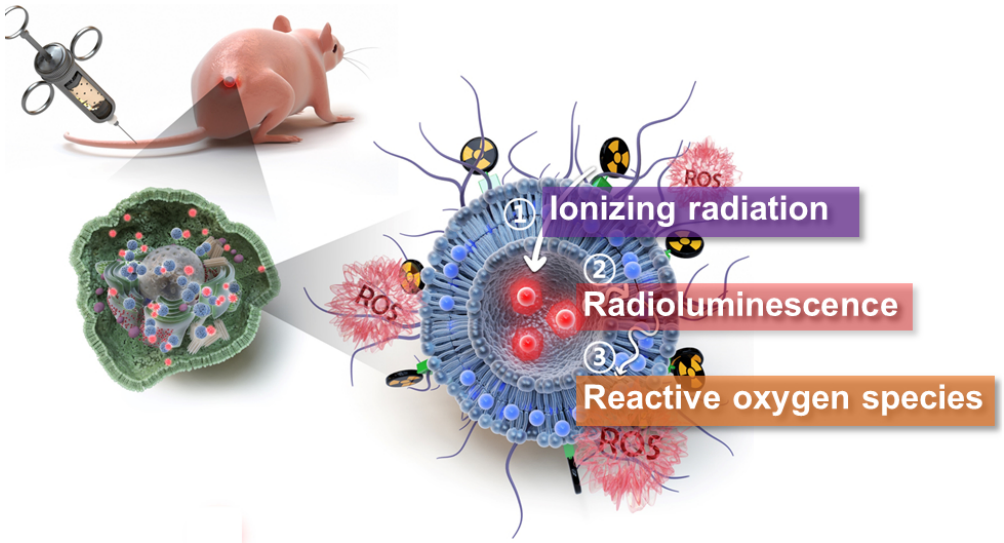

Table of Contents

82x44mm (300 x 300 DPI)

Europium-Diethylenetriaminepentaacetic Acid (Eu-DTPA) Loaded Radioluminescence Liposome Nano-Platform for Effective Radioisotope-Mediated Photodynamic Therapy

Wooseung Lee[1,], Miyeon Jeon[1,*], Jinyeong Choi[1], Chiwoo Oh[1], Gaeun Kim[1], Seongmoon Jung[1,2], Changsoon Kim[3,4], Sung-Joon Ye[1], Hyung-Jun Im[1,5]*

1. Department of Applied Bioengineering, Graduate School of Convergence Science and Technology, Seoul National University, Seoul (08826), Republic of Korea

2. Department of Radiation Oncology, Seoul National University Hospital, Seoul (03080), Republic of Korea

3. Department of Intelligence and Information, Graduate School of Convergence Science and Technology, Seoul National University, Seoul (08826), Republic of Korea

4. *Inter-University Semiconductor Research Center, Seoul National University, Seoul (08826), Republic of Korea*

5. Department of Molecular Medicine and Biopharmaceutical Sciences, Graduate School of Convergence Science and Technology, Seoul National University, Seoul (08826), Republic of Korea

* These authors contributed equally: Wooseung Lee, Miyeon Jeon

CORRESPONDING AUTHOR

Hyung-Jun Im, MD, PhD

Email: iiihjjj@gmail.com; iiihjjj@snu.ac.kr

Address: 18-dong, Gwanak-ro 1, Gwanak-gu, Seoul, Republic of Korea, (zip: 08826)

ABSTRACT

Photodynamic therapy (PDT) is an effective anti-cancer strategy with a higher selectivity and fewer adverse effects than conventional therapies; however, shallow tissue penetration depth of light has hampered the clinical utility of PDT. Recently, reports have indicated that Cerenkov luminescence -induced PDT may overcome the tissue penetration limitation of conventional PDT. However, the effectiveness of this method is controversial because of its low luminescence intensity. Herein, we developed a radiolabeled diethylenetriaminepentaacetic acid chelated Eu^{3+} (Eu-DTPA) / photosensitizer (PS) loaded liposome (Eu/PS-lipo) that utilizes ionizing radiation from radioisotopes for effective *in vivo* imaging and radioluminescence-induced PDT. We utilized Victoria blue-BO (VBBO) as a PS and observed an efficient luminescence resonance energy transfer between Eu-DTPA and VBBO. Furthermore, ^{64}Cu labeled Eu lipo demonstrated a strong radioluminescence with a two-fold higher intensity than Cerenkov luminescence from free ^{64}Cu. In our radioluminescence liposome, radioluminescence energy transfer (RET) showed a six-fold higher energy transfer efficiency to VBBO than Cerenkov luminescence energy transfer (CLET). ^{64}Cu labeled Eu/VBBO lipo (^{64}Cu-Eu/VBBO lipo) showed a substantial tumor uptake of up to 19.3 %ID/g by enhanced permeability and retention effects, as revealed by *in vivo* positron emission tomography. Finally, the PDT using ^{64}Cu-Eu/VBBO lipo demonstrated significantly higher *in vitro* and *in vivo* therapeutic effects than Cerenkov luminescence -induced PDT using ^{64}Cu-VBBO lipo. This study envisions a great opportunity for clinical PDT application by establishing the radioluminescence liposome which has high tumor targeting, and efficient energy transfer capability from radioisotopes.

KEYWORDS: photodynamic therapy; europium; radioluminescence; therapeutic; positron emission tomography

Photodynamic therapy (PDT) utilizes two non-toxic components, the photosensitizer (PS) and visible light, to eliminate cancer cells. Visible light at a specific wavelength can excite PS to generate reactive oxygen species (ROS) that can kill cancer cells. Photodynamic therapy is in the spotlight as one of the next generation anti-cancer therapeutics because it is non-invasive, has fewer side effects, and has been proven to be effective for early stage cancer treatment.[1, 2] It is currently used in the clinic for the treatment of various types of malignant diseases, including early stage esophageal cancer, lung cancer, head and neck cancer, and skin cancer.[3, 4]

Photodynamic therapy is not widely utilized in the clinical setting because of the limited tissue penetration depth of light and modest tumor targeting ability of PS.[5] Recently, X-ray-induced PDT was suggested to overcome the limitation of tissue penetration depth of light.[6] Instead of using an external visible light source, ionizing radiation can be used to generate visible light through nanoparticles (NP) containing scintillating materials, such as Europium (Eu) and Terbium (Tb).[6-8] However, X-ray-induced PDT may not be feasible in the clinical setting because the additional X-ray irradiation can only be applied to a limited number of lesions for a short period of time, and could be harmful to normal tissue.[7] However, Cerenkov luminescence emitted from particle radiation can also be used for induction of PDT in place of X-ray irradiation.[9-11] This radioisotope mediated PDT has advantages over X-ray-induced PDT in that it can treat multiple target lesions after intravenous injection and does not need an external beam irradiation.[11] Recently, Dalong *et al.* reported that Cerenkov-induced PDT using ^{89}Zr labeled magnetic NPs with porphyrin molecules exhibited excellent therapeutic effects.[10] However, Cerenkov luminescence is very dim, thus the clinical efficacy of this method is questionable; the energy of Cerenkov luminescence from ^{18}F comprises of less than 0.006% of the total energy released from the radioisotope.[12] Furthermore, a broad emission wavelength of Cerenkov luminescence could be a source of

ineffective energy transfer to PS.[13] In addition, previous studies have utilized hard-core NPs for the enhancement of PDT efficacy,[6, 9, 10, 14-17] which have the disadvantage of a low targeting efficiency that mainly stems from the non-specific interaction with serum proteins and recognition by reticuloendothelial system.[18] The hard-core NPs may also be toxic because they are chemically stable and difficult for lysosomes of the tissue macrophage system to digest.[19, 20]

Therefore, we developed a radiolabeled, Eu and PS co-loaded liposome nano-platform for radioisotope mediated *in vivo* imaging and PDT with the intention of combining the advantages of X-ray- and Cerenkov-induced PDT. We tried to overcome the limitation of X-ray-induced PDT by utilizing radioisotopes as an energy source, and the dim Cerenkov luminescence intensity by adding scintillating materials. First, diethylenetriamine pentaacetic acid (DTPA) chelated Eu^{3+} (Eu-DTPA) was loaded in the liposome for scintillation of ionizing radiation. Unlike previous approaches that utilized hard-core NPs with lanthanide doping for X-ray-induced PDT, we used a liposome nano-platform to ensure better biocompatibility.[21, 22] Furthermore, PS was loaded in the lipid bilayer of the liposome and ^{64}Cu was labeled onto the surface of the liposome to induce radioluminescence from Eu-DTPA. As a result, ionizing radiation from the labeled radioisotope interacted with Eu-DTPA and produced radioluminescence, the energy of which could be transferred to the PS to produce ROS for PDT. In addition, positron, radioluminescence, and characteristic X-ray from the nano-platform enabled multimodal imaging. The advantages of using radioluminescence over Cerenkov luminescence for PDT were then evaluated by comparing the radiolabeled PS loaded liposome nano-platforms with and without Eu-DTPA loading.

RESULTS AND DISCUSSION

Study Scheme

Our radioluminescence liposome nano-platform for PDT was designed to load Eu-DTPA in the hydrophilic core, PS in the hydrophobic lipid bilayer, and radioisotopes on the surface of the liposome. Rose Bengal (RB), Victoria blue-BO (VBBO), and chlorin e6 (Ce6) were tested for PSs. Europium-DTPA loaded liposome (Eu lipo), Eu-DTPA, and PS co-loaded liposome (Eu/RB lipo, Eu/VBBO lipo, Eu/Ce6 lipo) were prepared by self-assembly with phosphatidylcholine (PC) derivatives and cholesterol. Europium lipo, VBBO lipo, and Eu/VBBO lipo were radiolabeled using ^{64}Cu (^{64}Cu-Eu lipo, ^{64}Cu-VBBO lipo, ^{64}Cu-Eu/VBBO lipo), and they were tested for their radioluminescence effect and ROS generation ability. Subsequently, ^{64}Cu-Eu/VBBO lipo was tested for *in vitro* and *in vivo* PDT and *in vivo* positron emission tomography (PET) imaging was conducted with ^{64}Cu-Eu/VBBO lipo to determine its biodistribution and passive targeting efficiency in the mouse xenograft tumor model. The radioluminescence and ROS generation mechanism of our nano-platform for PDT can be explained as a 3-step event: First, Eu-DTPA emits radioluminescence in red visible spectrum (λ_{em}= 615 nm) by the labeled radioisotopes. Then the radioluminescence energy from the Eu-DTPA is transferred to the PS. Finally, PS emits ROS by radioluminescence energy transfer (RET) to kill tumor cells (**Figure 1**).

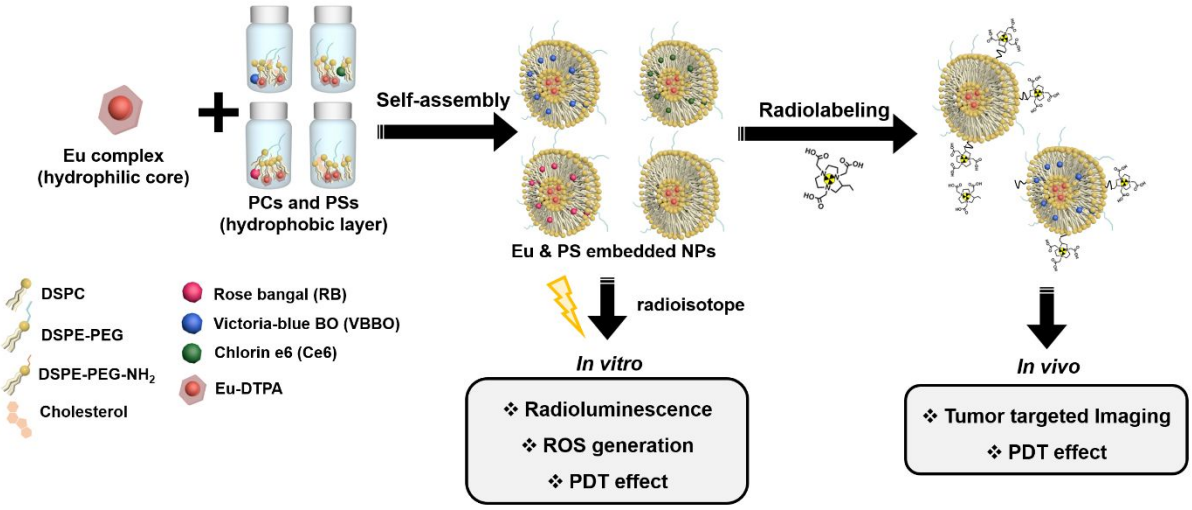

Figure 1. Schematic diagram of Eu/PS loaded radioluminescence liposome nano-platform synthesis and experimental design.

Size and Radiochemical Stability of Radiolabeled Eu/PS Lipo

The spherical shape and uniform size distribution of Eu/VBBO lipo were revealed by transmission electron microscopy (TEM) (**Figure 2a**). Hydrodynamic sizes of Eu lipo, Eu/RB lipo, Eu/Ce6 lipo, and Eu/VBBO lipo were 76.65 ± 22.88, 76.35 ± 26.58, 77.09 ± 27.64, and 78.14 ± 27.93 nm, respectively (**Figure 2b**). The stabilities of the liposome nano-platform in various physiological solutions (phosphate buffered saline (PBS), human serum, and cell media) were assessed to determine the feasibility of *in vivo* utilization of the liposome nano-platform. There were no visible aggregates or precipitates when used in the physiological solutions for 7 d (**Supporting Figure 1**). Additionally, the hydrodynamic sizes of the liposome nano-platform were stable for 14 d, which showed high *in vitro* stability of the nano-platform (**Figure 2c**). In further experiments, VBBO was chosen for the PS because it had the best matched absorbance wavelength (λ_{abs}= 615 nm) among the tested PSs with an emission wavelength of Eu (λ_{em}= 615 nm)

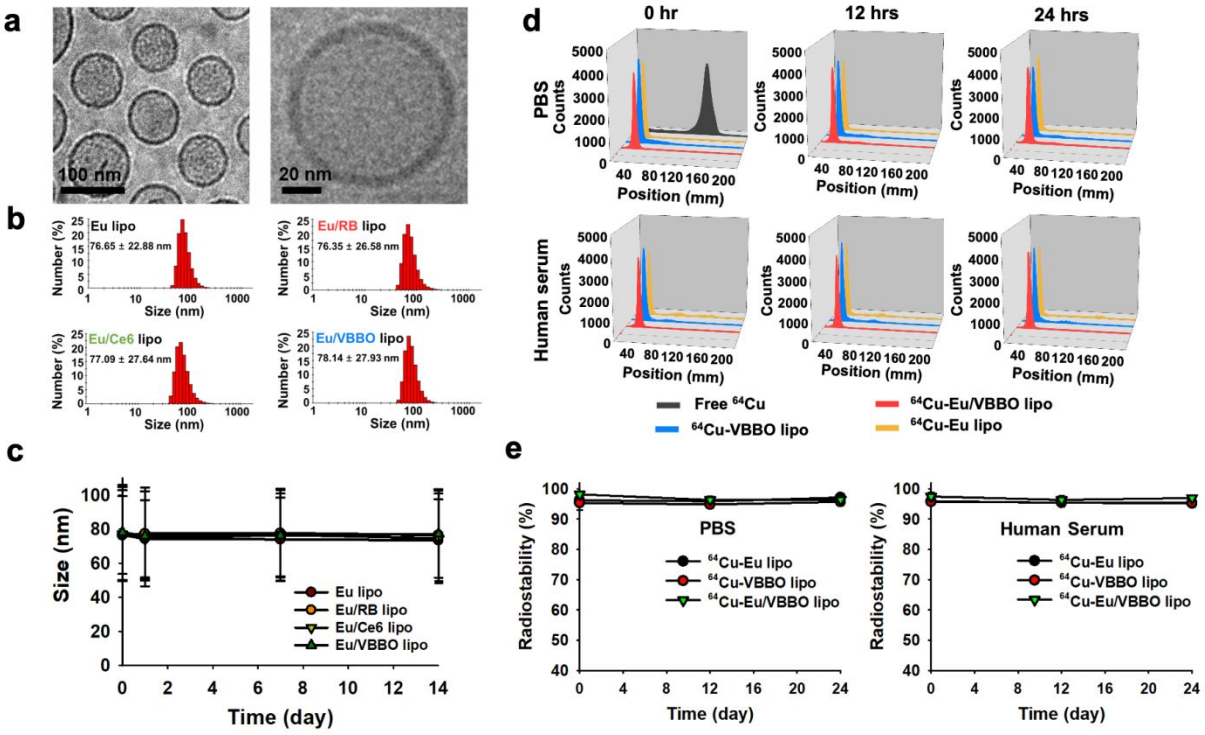

Figure 2. Characterization of Eu lipo and Eu/PS lipo. (a) TEM images of Eu/VBBO lipo with low (left) and high magnifications (right), respectively. (b) Hydrodynamic sizes of Eu lipo and Eu/PS lipo (n = 6, mean ± s.d.). (c) Stability test of Eu lipo and Eu/PS lipo in PBS for 14 d (n = 6, mean ± s.d.). (d) and (e) Radiolabeling stability test in PBS and human serum solutions (n = 6, mean ± s.d.). Eu: Eu-DTPA, PS: photosensitizer, RB: rose bengal, Ce6: chlorin e6, VBBO: victoria blue-BO.

(**Supporting Figure 2**). The radiolabeling efficiencies of ^{64}Cu-Eu lipo, ^{64}Cu-VBBO lipo, and ^{64}Cu-Eu/VBBO lipo were 96.2 ± 1.68%, 95.3 ± 2.33%, and 98.1 ± 0.68% in PBS, respectively (**Supporting Figure 3**). The radiochemical stabilities were over 95% for up to 24 h in PBS and human serum (**Figure 2d-e**). Thus, the radiolabeled Eu/PS loaded radioluminescence liposome nano-platform was very stable in physiological solution in terms of size and radiochemistry profile, which suggesting that *in vivo* utilization of the nano-platform would be effective.

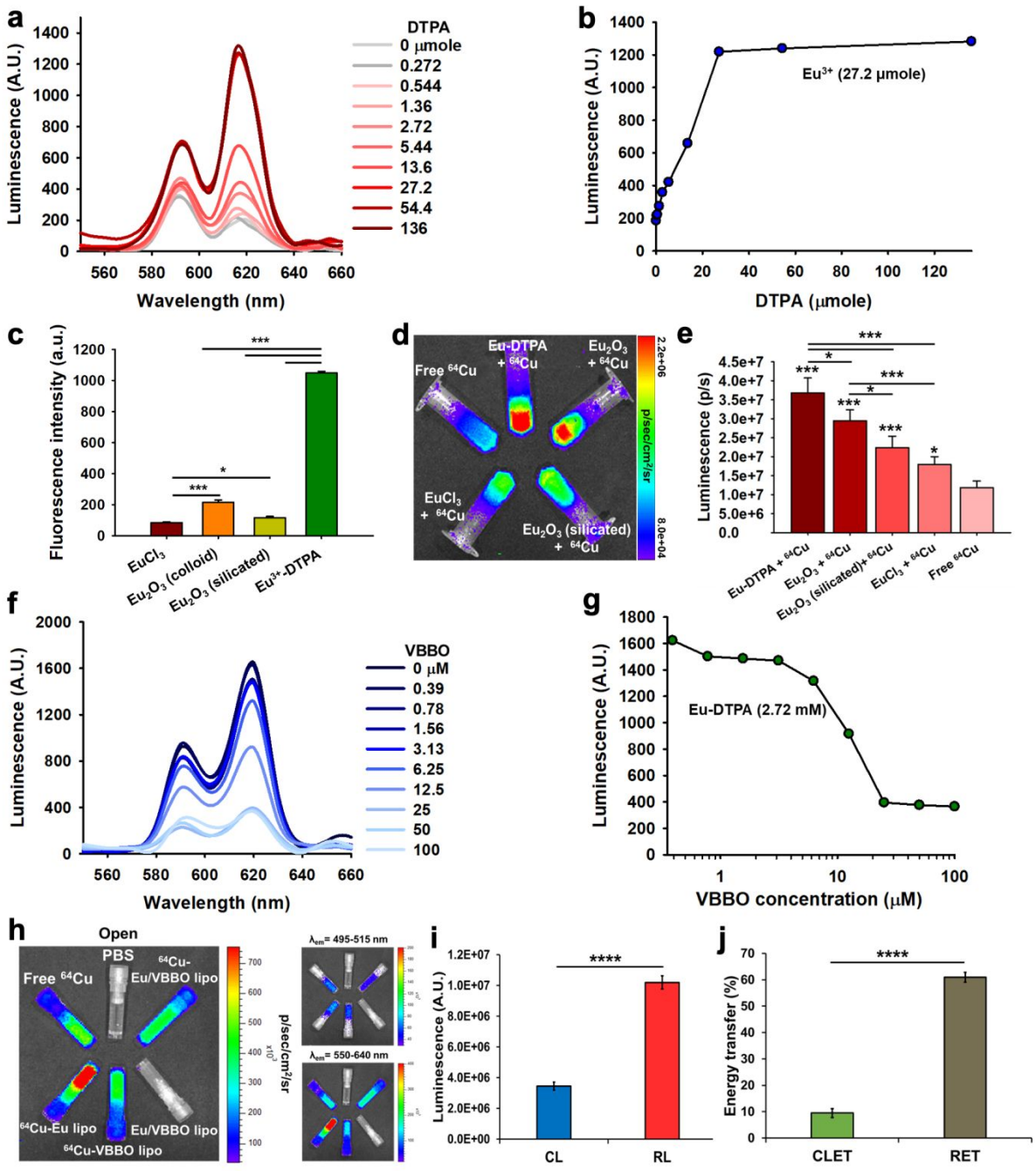

Figure 3. Radioluminescence and radioluminescence energy transfer. (a) and (b) Luminescence emission spectra of Eu^{3+} with the addition of diethylenetriamine pentaacetic acid (DTPA). (c) Luminescent intensities in different forms of Eu^{3+} included NPs (n = 5, mean ± s.d.). (d) and (e) Radioluminescence imaging and quantitative comparison with various Eu NPs in the presence of

^{64}Cu (500 μCi) (n = 5, mean ± s.d.). Notably, the amount of Eu was the same (13.6 μmol) in the various Eu containing NPs. (f) and (g) Emission spectra of Eu-DTPA by adding VBBO with constant Eu-DTPA (2.72 μmol) concentration. (h) Radioluminescence imaging in different kinds of liposomes with and without ^{64}Cu labeling under open, green, and red emission filters by IVIS. The activity of ^{64}Cu in free ^{64}Cu, ^{64}Cu-Eu lipo, ^{64}Cu-VBBO lipo, ^{64}Cu-Eu/VBBO lipo was the same (500 μCi). The concentration of VBBO in ^{64}Cu-VBBO lipo, ^{64}Cu-Eu/VBBO lipo, and Eu/VBBO lipo was the same (12.5 μM). The amount of Eu in ^{64}Cu-Eu lipo, ^{64}Cu-Eu/VBBO lipo, and Eu/VBBO lipo was the same (5.44 μmol) (i) Quantitative comparisons between Cerenkov luminescence (CL) and radioluminescence (RL) (n = 6, mean ± s.d.). (j) Quantitative comparisons between Cerenkov luminescence energy transfer (CLET) and radioluminescence energy transfer (RET) (n = 6, mean ± s.d.). *: $P < 0.05$, **: $P < 0.01$, ***: $P < 0.001$, ****: $P < 0.0001$. The one-way ANOVA followed by Tukey post hoc test for (c, e) and Student's t test for (i, j) were conducted for statistical analysis.

Radioluminescence and Radioluminescence Energy Transfer of Radiolabeled Eu/VBBO Lipo

We utilized Eu-DTPA for radioluminescence emission and confirmed that luminescence from Eu^{3+} was enhanced by chelation with DTPA in a dose dependent manner and saturated when the amount of Eu^{3+} and DTPA were the same (**Figure 3a-b**). Moreover, Eu-DTPA showed a significantly higher luminescence intensity under ultraviolet (UV) excitation than Eu_2O_3 NPs in colloid or silicated form, (5.1, 8.9 folds, respectively) (**Figure 3c, Supporting Figure 4**). When radioluminescence from the Eu-DTPA, Eu_2O_3 NPs, and Eu_2O_3 NPs (silicated) under ^{64}Cu were compared, the radioluminescence intensity of Eu-DTPA was significantly higher than Eu_2O_3 NPs, and Eu_2O_3 NPs (silicated) (**Figure 3d-e**). Furthermore, the radioluminescence intensity of the Eu-

DTPA was 7.16-fold higher than Eu_2O_3 NPs in colloid form and 8.9-fold higher than Eu_2O_3 NPs (silicated) in the presence of ^{99m}Tc (**Supporting Figure 7**).

Europium ion is a rare earth metal and has been used as a luminescent probe for various purposes because of its unique luminescence properties, including sharp emission bands, long luminescence life time, and large Stoke shift.[23-25] The luminescence of Eu^{3+} is emitted from the electronic 4f-4f transitions from the $^5D_0$ level to $^7F_{J=0,1,2,3,4}$ ground state and the transition of $^5D_0 \rightarrow {}^7F_2$ is responsible for the most intensive luminescence at 615 nm. In solution, Eu^{3+} emits a very low intensity luminescence because of the quenching effect of water molecules. To enhance the luminescence intensity, Eu^{3+} can be combined with chelators, such as DTPA derivatives or organic chromophores, including so called antenna like pyridine and bipyridine derivatives.[26-31] The luminescence intensity of Eu^{3+} can be enhanced by doping into hard-core NPs, such as sodium zinc molybdate NPs,[14] zinc oxide NPs,[32] yttrium oxide NPs,[33] and cerium oxide NPs.[34] The Eu^{3+} doped hard-core NPs or Eu_2O_3 NPs are reported to produce strong luminescence emissions by ionizing radiation, including X-ray, gamma and beta rays.[6, 35-38] Also, we found that Eu-DTPA showed the significantly higher radioluminescence than Eu_2O_3 NPs and Eu_2O_3 (silicated) NPs. We assume that the difference is caused by the concentration quenching effect in Eu_2O_3 NPs. Although the amount of Eu^{3+} was the same between the solutions containing Eu-DTPA and Eu_2O_3 NPs (13.6 μmol), Eu-DTPA is well dispersed in the solution while Eu_2O_3 NP has a high ion concentration in each NP (Calculated number of Eu^{3+} ions = 6.096×10^7 / NP, calculated from https://materialsproject.org/materials/mp-647924/). The concentration quenching effect of lanthanides based NPs has been reported in the literature.[39, 40] For example, Eu^{3+} doped alumina displayed a much longer luminescence lifetime than Eu_2O_3 NPs.[41]

It has been reported that the luminescence of Eu can be enhanced by chelation using chelators with or without chromophores.[42, 43] Chelator without chromophore can enhance the luminescence of Eu^{3+} because Eu^{3+} could be protected by the chelators from water molecules which can quench luminescence of Eu^{3+} dramatically by solvating Eu^{3+} in aqueous environment. Also, a chromophore in chelator can function as an 'antenna,' absorbing incident light then transferring this excitation to the Eu^{3+} ion to further enhance the luminescence of Eu^{3+}.[44] We used chelator without chromophore, DTPA, because DTPA is widely used chelator in the clinic based on its excellent safety profile. For example, Gd-DTPA is used for MRI contrast agent, and ^{99m}Tc-DTPA is used for renal function test in the clinic.

We found that Eu-DTPA had excellent radioluminescence abilities, and the emitted radioluminescence was sufficient for the successful *in vivo* PDT. Luminescence resonance energy transfer (LRET) between lanthanides, such as Eu^{3+} ion as a donor to the organic dyes or quantum dots as acceptors have been reported.[45, 46] We found that the luminescence intensity from Eu-DTPA could be efficiently reduced by adding VBBO, indicating the occurrence of LRET from Eu-DTPA to VBBO (**Figure 3f-g**). Assuming that the presence of VBBO did not introduce another nonradiative de-excitation pathway for Eu-DTPA in addition to LRET, the LRET efficiency was quantified as 1 – L/L0, where L is the luminescence intensity of Eu-DTPA in the presence of VBBO and L0 is the luminescence intensity of Eu-DTPA without VBBO.[47] From the results shown in **Figure 3g**, the LRET efficiency between Eu-DTPA and VBBO could reach up to 0.78.

After synthesis of Eu lipo, loading efficiency of Eu-DTPA was confirmed to be about 31% by measuring luminescence from purified and unpurified Eu lipo (**Supporting Figure 5**). The radioluminescence ability of Eu lipo was confirmed by adding ^{99m}Tc, which has no luminescence

itself. *In vivo* Imaging System (IVIS) imaging revealed that the radioluminescence was associated with ^{99m}Tc activity and Eu lipo concentration (**Supporting Figure 6**). Furthermore, Eu lipo emitted fluorescence X-rays *via* de-excitation processes caused by the interaction between external X-rays and Eu. Thus, Eu lipo can be imaged by an in-house X-ray fluorescence (XRF) imaging device (**Supporting Figure 8**).[48] These results suggest that radiolabeled Eu lipo could be used as a multimodal imaging agent, including PET, X-ray fluorescence imaging, multispectral SPECT imaging and radioluminescence imaging.[37] We were also able to measure the amount of Eu^{3+} in Eu/VBBO lipo by the K-shell X-ray fluorescence (XRF) detection system (**Supporting Figure 9**).

To the radioluminescence liposome nano-platform, ^{64}Cu was labeled for further *in vivo* imaging and therapy experiments. After radiolabeling of ^{64}Cu to the radioluminescence liposome nano-platform, luminescence imaging of the free ^{64}Cu, ^{64}Cu-Eu lipo, ^{64}Cu-VBBO lipo, Eu/VBBO lipo, ^{64}Cu-Eu/VBBO lipo and PBS were performed using IVIS. We found that luminescence emitted by ^{64}Cu-Eu lipo was significantly higher than free ^{64}Cu (**Figure 3h**). We compared the intensity of radioluminescence from the Eu-DTPA in ^{64}Cu-Eu lipo, quantified by the luminescence of ^{64}Cu-Eu lipo minus that of free ^{64}Cu, with the intensity of the Cerenkov luminescence from free ^{64}Cu and found that the radioluminescence was higher than the Cerenkov luminescence by more than a factor of 2 ($3.44 \times 10^6 \pm 2.6 \times 10^5$ p/s *vs*. $1.02 \times 10^7 \pm 4.30 \times 10^5$ p/s, $P < 0.0001$) (**Figure 3i**). We also found that the luminescence intensity of ^{64}Cu-VBBO was lower than that of free ^{64}Cu, and the intensity of ^{64}Cu-Eu/VBBO lipo was lower than that of ^{64}Cu-Eu lipo (**Figure 3h**). These results indicate that VBBO co-loading can induce energy transfer to VBBO from Cerenkov luminescence or radioluminescence. Cerenkov luminescence from free ^{64}Cu showed a higher intensity at the red visible light region (550~640 nm wavelength) than the blue light region (400~450 nm) (**Figure 3h, Supporting Figure 10**), because of the rapid light shift of Cerenkov luminescence.[13] The

quantified Cerenkov luminescence energy transfer (CLET) and RET were compared and we found that RET of ^{64}Cu-Eu/VBBO lipo was about six-fold higher than CLET of ^{64}Cu-VBBO lipo (9.5 ± 1.69 % *vs*. 61.0 ± 1.87 %, P < 0.0001) (**Figure 3j**). The Förster radii between Eu-DTPA (donor) and various dyes (acceptor) have been reported to range from 5 to 10 nm.[46] Since the diameter of our liposome nano-platform is 78 nm, it is likely that an appreciable amount of VBBO (acceptor) was present within the Förster radius of Eu-DTPA in ^{64}Cu-Eu/VBBO lipo. As a result, the calculated RET efficiency in our liposome nano-platform (64.2%) is high, approaching the calculated maximum LRET efficiency between Eu-DTPA and VBBO (78%) in solution (**Figure 3g**), and is much larger than the efficiency of the ^{64}Cu-to-VBBO CLET (9.5%). It is unclear whether the CLET occurs by radiative energy transfer, *i.e.*, *via* absorption of photons emitted by Cerenkov luminescent, or resonantly, analogous to LRET. In either case, the lower efficiency of the CLET compared to the RET can be rationalized; in general, radiative energy transfer is much less efficient than resonant energy transfer;[49] the Eu-DTPA emission spectrum, compared to broad Cerenkov luminescence, has a sharper peak and a better spectral matching with the VBBO absorption spectrum. Based on these results, we hypothesized that radioluminescence-induced PDT by ^{64}Cu-Eu/VBBO lipo will be more effective than Cerenkov luminescence-induced PDT by ^{64}Cu-VBBO lipo.

Effective ROS Generation and *In Vitro* PDT Effect of ^{64}Cu-Eu/VBBO Lipo

Reactive oxygen species generation and *in vitro* PDT tests were conducted using ^{64}Cu-Eu/VBBO lipo and ^{64}Cu-VBBO lipo; all studies were triplicated. Free ^{64}Cu or ^{64}Cu-Eu lipo were utilized as the control group. Singlet oxygen was detected by measuring a fluorescence of Singlet Oxygen Sensor Green (SOSG) reagent. In ^{64}Cu-VBBO lipo, the ROS levels with 100 and 200 μCi of ^{64}Cu,

were 3.10 and 10.11 times higher than those with 0 μCi of ^{64}Cu, respectively ($P < 0.01$ and $P < 0.001$, respectively). In 30 μCi of ^{64}Cu, ^{64}Cu-VBBO lipo could not generate ROS, but ^{64}Cu-Eu/VBBO lipo could. The ROS fold increases of ^{64}Cu-Eu/VBBO lipo were significantly higher than those of ^{64}Cu-VBBO lipo at all ^{64}Cu activity points ($P < 0.001$). Free ^{64}Cu did not produce ROS up to 200 μCi (**Figure 4a**). ROS generation in the FaDu cells after incubation with ^{64}Cu-Eu/VBBO lipo was also confirmed using the CellROX® reagent *via* the fluorescence microscopic image (**Figure 4b**). *In vitro* PDT effects of ^{64}Cu-Eu lipo, ^{64}Cu-VBBO lipo, and ^{64}Cu-Eu/VBBO lipo were compared in the FaDu cell line (a human head and neck cancer cell line), by 3-(4,5-dimethylthiazol-2-yl)-2,5-diphenyltetrazolium bromide (MTT) assay. ^{64}Cu-VBBO lipo and ^{64}Cu-Eu/VBBO lipo showed tumor cell killing effects with ^{64}Cu activity of 30 and 100 μCi. ^{64}Cu-Eu lipo showed no significant cell killing effects. The cell killing effect was significantly higher in ^{64}Cu-Eu/VBBO lipo than ^{64}Cu-VBBO lipo (30 μCi ($P < 0.05$), 100 μCi ($P < 0.05$)) (**Figure 4c**). Cell microscopic images after MTT assay were corroborated with the quantified results of MTT assays (**Figure 4d**). Thus, ^{64}Cu-Eu/VBBO lipo had a higher ROS generation ability and *in vitro* PDT effect than ^{64}Cu-VBBO lipo, suggesting that radioluminescence-induced PDT was more efficient than Cerenkov luminescence-induced PDT.

It is noteworthy that ^{64}Cu has 38% of beta ray emissions, which is a type of cancer therapeutic ionizing radiation.[50] We found that there was neither ROS generation nor PDT effect under 200 μCi of free ^{64}Cu, but we were able to observe significant ROS generation and PDT effect with only one seventh (30 μCi) of ^{64}Cu with the addition of our radioluminescence liposome nano-platform in *in vitro* PDT experiments. This indicates that our radioluminescence nano-platform could be applied to enhance the treatment effect or lower the radiation dose of currently used targeted radioisotope therapy using beta ray emitters. Furthermore, ^{99m}Tc, a pure gamma ray emitter, which

is used for *in vivo* imaging,[51-53] was able to induce ROS generation from Eu/PS lipo (**Supporting Figure 11**), which further suggests the possibility of converting diagnostic radioisotopes into therapeutics by the addition of a radioluminescence liposome nano-platform.

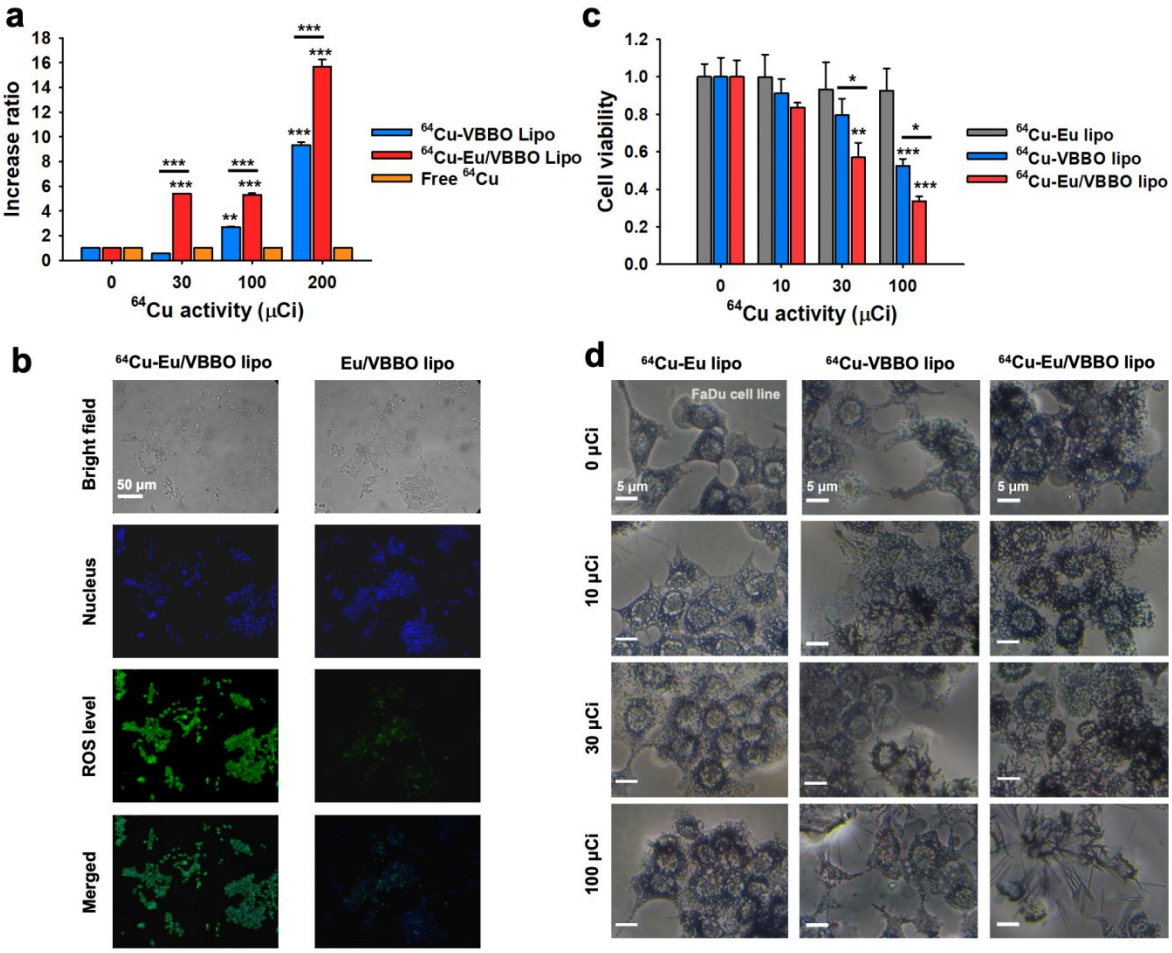

Figure 4. ROS generation test and *in vitro* radioisotope-induced photodynamic therapy. (a) ROS generation by ^{64}Cu-Eu/VBBO lipo, ^{64}Cu-VBBO lipo, and free ^{64}Cu (n = 6, mean ± s.d.) at different activities of ^{64}Cu. (b) Fluorescence microscopic image of FaDu cells after incubation with ^{64}Cu-Eu/VBBO lipo or Eu/VBBO lipo (^{64}Cu activity: 100 μCi, Green: CellROX® for ROS detection, Blue: Hoechst 33342 for cell nuclei staining, scale bar: 50 μm). (c) Tumor cell killing effect of ^{64}Cu-Eu lipo, ^{64}Cu-VBBO lipo, and ^{64}Cu-Eu/VBBO lipo at different activities of ^{64}Cu (n = 6, mean

± s.d.). (d) Microscopic cell images of ^{64}Cu-Eu lipo, ^{64}Cu-VBBO lipo, and ^{64}Cu-Eu/VBBO lipo at different activities of ^{64}Cu after the *in vitro* PDT (Scale bar: 5 μm). *: $P < 0.05$, **: $P < 0.01$, ***: $P < 0.001$. The one-way ANOVA followed by Tukey post hoc test was conducted for statistical analysis.

Efficient Tumor Targeting by EPR Effect

In vivo positron emission tomography (PET) imaging was performed to demonstrate the imaging ability of ^{64}Cu-Eu/VBBO lipo and confirm the passive targeting efficiency of the NPs in FaDu xenograft tumor mouse model (**Figure 5a**). The image revealed the substantially long circulation half-life and efficient tumor targeting ability of ^{64}Cu-Eu/VBBO lipo. Quantified PET uptakes of major organs are shown in **Figure 5b**. The uptake of the tumor gradually increased to 19.29 ± 4.70 %ID/g 48 h after the injection. The circulation half-life of ^{64}Cu-Eu/VBBO lipo was 20.15 h (**Figure 5c**). Tumor to background (muscle, blood pool, and liver) ratios increased gradually over time until 48 h after the injection up to 16.77, 2.53, and 0.55 folds, respectively (**Figure 5d-f**). Additionally, ^{64}Cu-VBBO lipo showed a similar biodistribution with ^{64}Cu-Eu/VBBO lipo, and there was no significant difference regarding tumor uptake between ^{64}Cu-VBBO lipo and ^{64}Cu-Eu/VBBO lipo at all time points ($P = 0.07$, 0.788, 0.688, 0.625, and 0.237) (**Supporting Figure 12**).

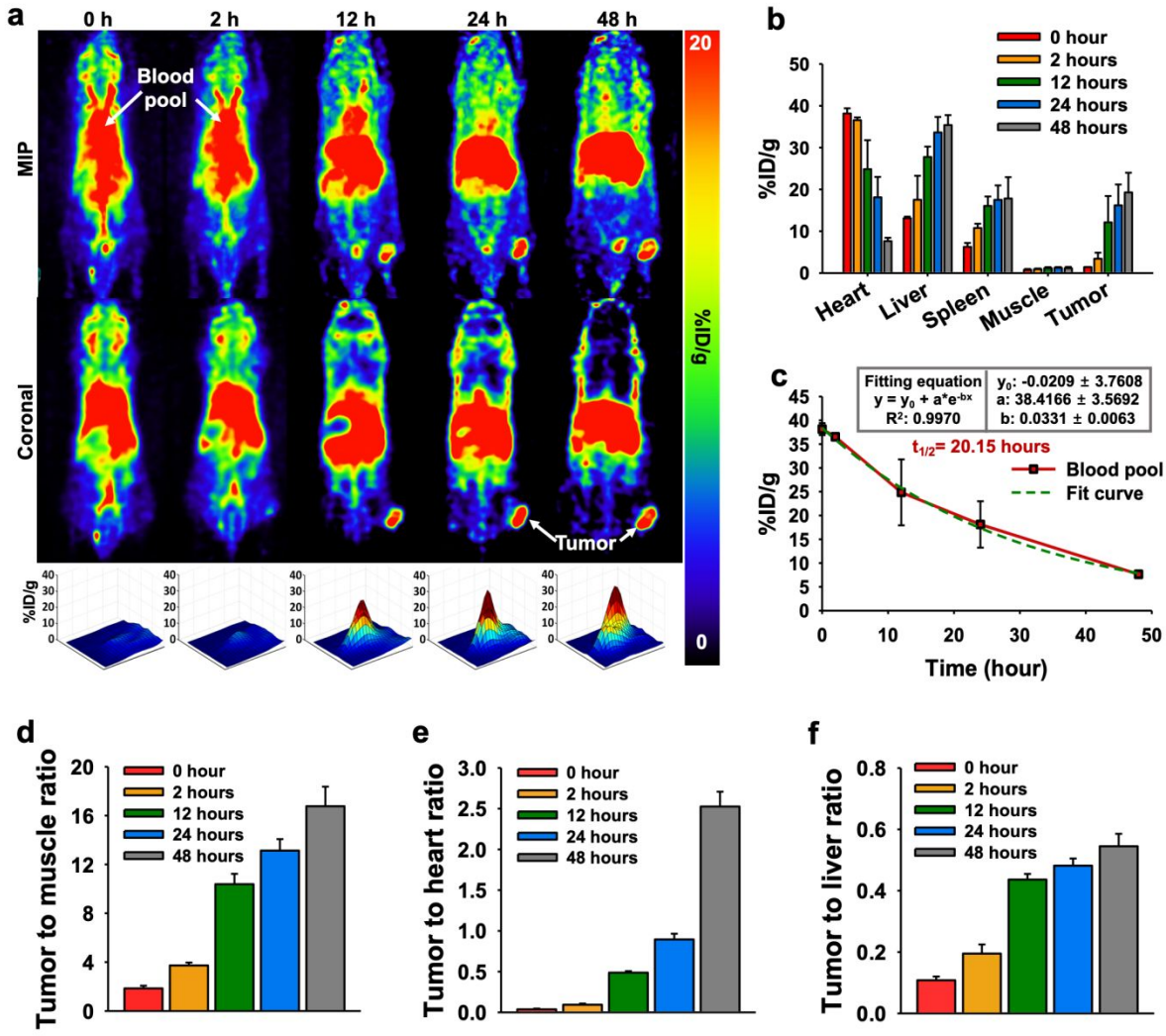

Figure 5. *In vivo* PET imaging and quantitative analysis for assessment of passive targeting efficiency of ^{64}Cu-Eu/VBBO lipo. (a) PET images of FaDu tumor bearing xenograft mouse model (n = 4) at different time points (0, 2, 12, 24, and 48 h) after intravenous injection of ^{64}Cu-Eu/VBBO lipo (upper row: maximal intensity projection (MIP), middle row: coronal, lower row: surface plot for the tumor area from the coronal image, z axis: %ID/g). (b) Quantification analysis of various organs and tumors at each time point (n = 4, mean ± s.d.). (c) Time activity curve of the blood pool and circulation half-life (n = 4, mean ± s.d.). (d), (e), and (f) Tumor targeting efficiency compared to 3 non-target areas (muscle, heart and liver) (n = 4, mean ± s.d.).

X-ray-induced PDT and Cerenkov luminescence-induced PDT have been shown to have good therapeutic effects in previous studies.[6, 9, 10, 14] However, these NPs were injected intratumorally in most of the studies probably because of their low tumor targeting efficiency.[6, 9, 14, 16] Kotagiri *et al.* reported that intravenously injected nanomicelles containing PS were utilized for Cerenkov radiation induced therapy. Although the quantitative tumor targeting efficiency was not reported, the circulation half-life of the nanomicelles was shorter than that of our liposome nano-platform (123 min *vs*. 20 h).[54] In a recent study, magnetic NPs were intravenously injected for Cerenkov luminescence induced PDT and the tumor uptake was around 5 %ID/g without targeting and 15.2 %ID/g with the application of an additional magnetic field.[10] We utilized a PEGylated liposome-based nano-platform for enhanced EPR effects and found that our liposome nano-platform had an excellent tumor targeting efficiency (~ 19 %ID/g) without any additional targeting strategy.

Effective *In Vivo* PDT of ^{64}Cu-Eu/VBBO Lipo

In vivo PDT was conducted by intravenous injection of ^{64}Cu-Eu/VBBO lipo (n = 4) and ^{64}Cu-VBBO lipo (n = 4) in a FaDu xenograft tumor mouse model. Normal saline (n = 4) and Eu/VBBO lipo (n = 4) were injected and these groups were used as the control groups. The ^{64}Cu-VBBO lipo and ^{64}Cu-Eu/VBBO lipo groups had higher therapeutic effects than the control groups. Furthermore, the ^{64}Cu-Eu/VBBO lipo had a better therapeutic effect than the ^{64}Cu-VBBO lipo group (**Figure 6a-c**). Thus, radioluminescence-induced PDT with ^{64}Cu-Eu/VBBO lipo had a higher tumor growth suppression ability than Cerenkov luminescence-induced PDT effect with ^{64}Cu-VBBO lipo *in vivo*. This difference can be attributed to the difference in efficiency between RET and CLET, because there was no significant difference in tumor uptake between ^{64}Cu-Eu/VBBO lipo and ^{64}Cu-VBBO lipo (**Supporting Figure 12**). Major organs and tumor tissues

were collected 48 h after intravenous injection of ^{64}Cu-Eu/VBBO lipo. No significant histologic damage was found in the heart, liver, spleen and thigh muscle on histological observation (**Figure 6c**).

The effectiveness of PDT is normally determined by the targeting efficiency of PS, oxygen concentration of tissue and delivered energy of light.[55] The PS delivery system has been extensively studied and includes liposome based, polymer, silica, gold, and iron oxide NPs.[56, 57] In our system, we utilized a PEGylated liposome nano-platform for efficient tumor targeting and we found that the tumor uptake of our nano-platform reached up to 19 %ID/g. This targeting efficiency is considerably high, within top 10%, compared to the previously reported targeting efficiencies of various NPs especially with or without targeting moieties (median = 3.17 %ID/g) (**Supporting Figure 13-14**).[58] The effect of PDT is also dependent on the dose of light (J/cm^2), which is calculated by the multiplication of irradiance (W/cm^2) and time (second).[59] Currently two types of ionizing radiation-induced PDT strategies, X-ray- and radioisotope-induced PDT, are under investigation. The dose of light for these methods are dependent on the radiation dose. X-ray-induced PDT has the advantage of providing a high radiation dose at tumor focus within a short duration of time (1 ~10 Gy per minute).[11] However, such a large amount of energy may be harmful to the surrounding normal tissue, and the high fluence of radioluminescence from the NPs may deplete the oxygen within the tumor, which will lead to the decreased efficiency of the PDT. However, radioisotope-induced PDT has the advantage of an emission of low fluence rates of light over a long period of time (half-lives of the utilized radioisotopes for PDT: ^{64}Cu = 12.7 h, ^{89}Zr = 78.4 h, ^{18}F = 110 min).[60] Previous studies on radioisotope-induced PDT have focused on the Cerenkov luminescence-induced PDT.[37, 54, 61] In our study, we utilized the scintillating Eu-DTPA for radioluminescence-induced PDT and found that the radioluminescence had a 2-fold higher

luminescence intensity and a transfer efficiency that was 6-fold higher in radioluminescence than Cerenkov luminescence (65% *vs*. 11%) mainly because of the efficient resonance energy transfer in RET. Thus, we believe radioluminescence-induced PDT holds promise for future ionizing radiation-induced PDT.

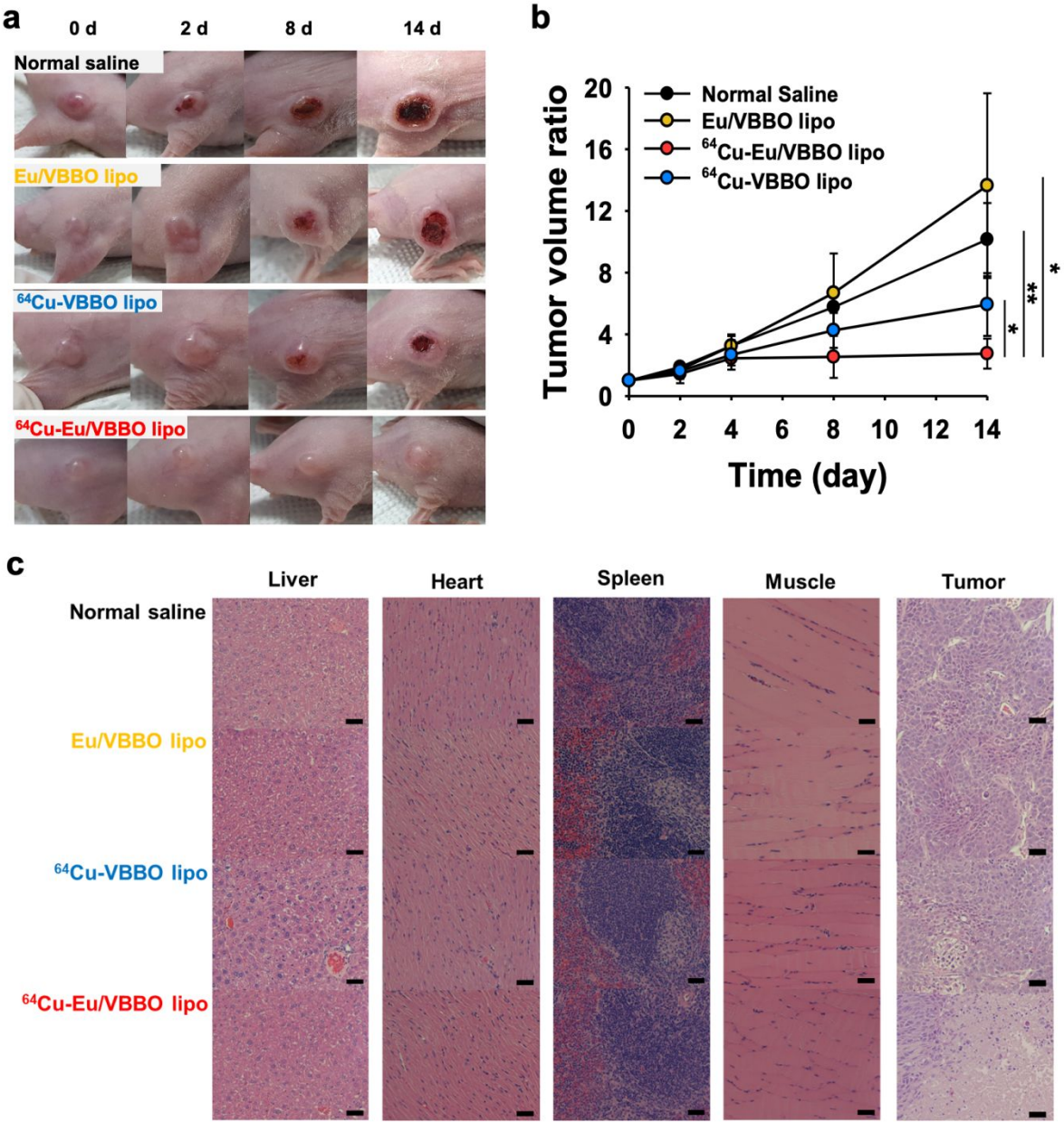

Figure 6. *In vivo* photodynamic therapy. (a) Tumor follow-up images in FaDu tumor bearing xenograft mouse model after intravenous injection of ^{64}Cu-Eu/VBBO lipo (n = 4), ^{64}Cu-VBBO lipo (n = 4), Eu/VBBO lipo (n = 4), or normal saline (n = 4). (b) Tumor volume ratio after the treatments (mean ± s.d.). *: $P < 0.05$, **: $P < 0.01$. The Student's t test was conducted for statistical analysis. (c) H&E stained major organs and tumor histological images at 14 d after the treatments.

Recently, there has been huge success in targeted radioisotope therapy in neuroendocrine tumor and castration resistant prostate cancer. In 2017, a phase 3 trial of ^{177}Lu-DOTATATE (Lutathera) for midgut neuroendocrine tumors showed markedly longer progression-free survival than octreotide treatment.[62] Furthermore, ^{177}Lu-PSMA agents have shown significantly better therapeutic effects than the other third line therapeutics for castration resistant prostate cancer.[63] These therapeutic radioisotope based therapeutics are found to be very effective, but have adverse effects including nephrotoxicity, hematologic toxicity, and salivary gland dysfunction caused by high radiation doses.[62-64] Radioisotopes for imaging purpose, such as ^{64}Cu and ^{99m}Tc, can exert PDT effects by combination with our radioluminescence PS loaded liposome nano-platform. In this study we created a radioluminescence liposome nano-platform that could be combined with radioisotope-based therapy to reduce adverse effects of therapeutic radioisotopes by reducing the dose or using the less toxic diagnostic radioisotope for the therapy.

We explored if Eu^{3+} caused toxicity *in vivo*. The intraperitoneal LD50 of $EuCl_3$ is 550 mg/kg.[65] Also, Ogawa *et al.* reported that no-observed-effect level of $EuCl_3$ is 200 mg/kg/day.[66] In our experiment, Eu^{3+} was used 40 mg/kg in mouse, which is one fifth of the no-observed-effect dose. Furthermore, Eu^{3+} was chelated by DTPA in our experiment. It is known that lanthanide chelates are less toxic than lanthanide ions. For example, the toxicity of $ScCl_3$ is dramatically reduced when it is chelated with EDTA (LD50: $ScCl_3$ = 24, Sc-EDTA = 108 mg).[14] Also, Gd ion is toxic but Gd-

chelates are safely used in the clinic for MRI contrast agents (LD50 of Gd is 0.5 mmol/kg while that of Gd-DTPA is 10 mmol/kg).[67, 68] We further explored the metabolism of Eu^{3+} using Inductively Coupled Plasma Mass Spectrometry (ICP-MS) in the major organs at 2 and 14 days after the intravenous injection of Eu/VBBO lipo (Eu^{3+} = 40 mg/kg). On day 2, ICP-MS measured Eu concentrations of liver (298.67 ± 82.86 ppm) and spleen (189.33 ± 22.14 ppm) were similar with the calculated concentration of Eu from the %ID/g in PET imaging (283.04 ± 8.81 ppm and 142.64 ± 23.72 ppm, respectively). On day 14, Eu concentrations of the liver and spleen dramatically decreased to less than one hundredth and one thirtieth, respectively, compared to those on day 2. Also, Eu element was found in the kidney on day 2 but not detectable on day 14 (**Supporting Figure 15**). Thus, we assume that the Eu-DTPA was excreted efficiently through kidney after dissociation from the injected Eu/VBBO lipo.

Furthermore, the hepatic and renal toxicity of Eu/VBBO lipo were also assessed by measuring the blood urea nitrogen (BUN), creatinine (Cr), alanine transaminase (ALT) and aspartate transaminase (AST) 14 days after injection of Eu/VBBO lipo (Eu^{3+} = 40 mg/kg) or normal saline in the normal BALB/c nude mouse (n = 4, and 4, respectively). The measured BUN, Cr, ALT and AST of all mice were within the normal range and there was no significant difference between saline and Eu/VBBO lipo injected groups, indicating that there is no observable renal or hepatic toxicity by Eu/VBBO lipo injection (**Supporting Figure 16**).

Although we observed no overt tissue or biochemical toxicity in the major organs in our experiment, it is possible that ^{64}Cu-Eu/VBBO lipo accumulation may damage normal tissue. Thus, dividing switch (radiolabeled targeting tracer) and effector (Eu/PS lipo) may provide further merits regarding the safe utilization of the radioluminescence liposome nano-platform. One potential approach would be the combination of radioluminescence / PS liposome nano-platform (effector)

with established immunoPET agents (switch) to convert diagnostic PET agents into therapeutics. In this study, the liposome nano-platform was produced by film method followed by sonication which is hard to be scaled-up.[69] The strategies for the large-scale production of the nano-platform is warranted for the future translational research.

CONCLUSION

We developed, here, an Eu-DTPA and PS loaded liposome nano-platform for effective *in vivo* imaging and radioisotope-induced PDT. We found that our liposome nano-platform presented 1) strong radioluminescence and characteristic X-ray emission, 2) efficient energy transfer from Eu-DTPA to PS, 3) high tumor targeting efficiency, and 4) effective ROS generation and *in vitro*/*in vivo* PDT effect. Furthermore, we found that radioluminescence-induced PDT was superior to Cerenkov-induced PDT in our experimental setting. Thus, our nano-platform may be a promising tool for radioisotope-induced PDT. We expect that our liposome nano-platform can be further utilized to enhance the efficacies of X-ray therapy or targeted radioisotope therapy.

METHODS

Materials

Cholesterol, Europium chloride · $6H_2O$, Rose bengal, victo-ria blue-BO, Europium oxide (< 150 nm), and diethylene-triaminepentaacetic acid (DTPA) were purchased from Sigma-Aldrich (Missouri, USA). 1,2-distearoyl-sn-glycero-3-phosphocholine (DSPC) and 1,2-distearoyl-sn-glycero-3-phosphoethanolamine-N-[amino(polyethylene glycol)-2000] (DSPE-PEG(2000)-NH2) were purchased from Avanti Polar Lipid, Inc (Alabama, USA). 1,2-distearoyl-sn-glycero-3-phosphoethanolamine (meyhoxy(polyethyleneglycol)-5000) (DSPE-mPEG(5000)) was purchased from Creative PEGWorks (North Carolina, USA). Chlorin e6 was purchased from Cayman Chemical (Michigan, USA). Dimethyl sulfoxide (DMSO) was obtained from DAEJUNG CHEMICALS & METALS Co., Ltd (Busan, Korea). 2-(p-Isothiocyanatobenzyl)-1,4,7-triazacyclononane-N,N',N,''-triacetic acid trihydrochloride ((p-SCN-Bn)-NOTA) was also purchased by FUTURECHEM (Seoul, Korea).

Instruments

All sizes of Eu/PS liposomes were measured using a dynamic light scattering instrument (DLS, ZETASIZER Nano ZS, Malvern Instrument Ltd., Worcestershire, UK). The TEM images of the liposomes were obtained using a Transmission Electron Microscope (TEM, TALOS L120C, FEI company, Oregon, USA) to confirm their morphologies and sizes. Fluorescence and absorbance signals were obtained using a microplate reader (SYNERGY H1, BioTek, Vermont, USA). For *in vitro* and *in vivo* Cerenkov and radioluminescence imaging, the *in vivo* imaging system (IVIS 100, Perkin Elmer, Massachusetts, USA) was used. The PET images were acquired by a PET scanner (GENISYS4, Sofie Bioscience, California, USA) after intravenous injection of ^{64}Cu labeled Eu lipo, VBBO lipo and Eu/VBBO lipo in tumor bearing mice.

Eu^{3+} Chelation with Diethylenetriaminepentaacetic acid (DTPA): Eu-DTPA Complex

$EuCl_3 \cdot 6H_2O$ and DTPA were dissolved in distilled water and 0.5 M NaOH solution, respectively. After dissolution and mixing with equal molar ratios, a solution together with Eu^{3+} and DTPA was adjusted to neutral pH and filtered by the size exclusion chromatographical method.

Eu-DTPA and Photosensitizer (PS) Loaded Liposome Preparation

A facile self-assembly method with phosphatidylcholine (PC) series and cholesterol was used for making a liposome structure. Phosphatidylcholines, 1,2-Distearoyl-sn-glycero-3-phosphocholine (DSPC), 1,2-distearoyl-sn-glycero-3-phosphoethanolamine-N-[methyl(polyethylene glycol)-5000] (ammonium salt) (DSPE-PEG(5000)-CH_3), and cholesterol were dissolved in chloroform at a 6.6:1.3:1.6 molar ratio. Subsequently, the PS was added in a lipid pre-mixture. Chloroform in the lipid phase solution was evaporated with a rotary evaporator until a transparent lipid thin layer coated the bottom of the *via*l. Following evaporation, the lipid layer was vacuumed for 12 h to remove the remaining residual chloroform inside the layer. Europium-DTPA complex solution was added to the lipid layer *via*l and sonicated to form multilamellar vesicles (MLVs). The MLVs solution was subjected to additional ultrasonication for 10 min. Then, a transparent liposome solution was filtered with a 0.2-μm pore syringe filter and 30 K molecular weight cut-off (MWCO) tube for further studies.

Characterization of Eu/PS Lipo with TEM and DLS

Europium/PS lipo was acquired by the TEM to confirm its morphology. For cryo-TEM imaging, the liposome was diluted with PBS solution before sample preparation onto a grid. The hydrodynamic size of the liposome was measured by the DLS instrument.

Radiolabeling of Eu and Ps Embedded Liposome (Eu/PS lipo) for *In Vivo* Imaging

For radiolabeling, 1,4,7-Triazacyclononane-1,4,7-triacetic acid (NOTA) was utilized as a chelator and 1,2-distearoyl-sn-glycero-3-phosphoethanolamine-N-[amino(polyethylene glycol)-2000] (ammonium salt) (DSPE-PEG(2000)-amine) was reacted with 2-(p-Isothiocyanatobenzyl)-1,4,7-triazacyclononane-N,N',N,''-triacetic acid trihydrochloride ((p-SCN-Bn)-NOTA) overnight. The NOTA modified DSPE-PEG (2000) was added to the lipid pre-mixture before the transparent lipid layer was prepared. This step was the same as the Eu/PS lipo preparation procedure. For the radiolabeling, radioisotope solution was adjusted to pH 5 using 0.5~1 M HCl solution and was mixed with NOTA modified Eu/PS lipo at 37℃ for 30 min. After the reaction, a radioisotope labeled Eu/PS lipo was eluted using a PD-10 column to purify it from unchelated free radioisotopes. To travel up-ward onto an ITLC-SG paper, 2 μL of radiolabeled lipo-some was loaded. The radioisotope was read onto the paper by measuring its radioactivity signal.

***In Vitro* Stability Test of Eu/PS Lipo**

Stability tests of liposomes loaded with Eu and PSs were conducted in PBS, human serum, and cell media (RPMI 1640) for 7 d. These lipo series were evaluated by measuring their sizes with DLS for up to 14 d to prove their stabilities in 3 different kinds of physiological conditions.

Eu^{3+} Quantification Analysis by K-shell X-ray Fluorescence (XRF) Detection System

The K-shell XRF detection system consisted of an external polychromatic X-ray source (X-RAD 320, Precision X-ray Inc., North Branford, CT, USA), a cadmium telluride (CdTe) detector for X-ray spectroscopy (X-123CdTe, Amptek Inc., Bedford, USA), and a cylindrical lead collimator. Six Eu-DTPA samples with different concentrations were used to obtain a linear relationship between the concentrations of Eu^{3+} and the amount of K-shell XRF photons emitted from Eu-DTPA. The concentrations of the samples were 0.058 wt/v %, 0.116 wt/v %, 0.233 wt/v %, 0.465 wt/v %, 0.93 wt/v %, and 1.86 wt/v %. Each sample was irradiated for 1 min by 140 kVp X-rays and the amount

of photon counts of the most dominant XRF peaks (Kα1 peak of 41.5 keV and Kα2 peak of 40.9 keV) from the measured X-ray spectra by the CdTe detector were quantified. The measurement was repeated 5 times for each sample. The calibration curve showed a good linear fit between the concentration and the amount of XRF photons counts (*i.e.*, $R^2 = 0.9989$). The XRF photon counts emitted from Eu^{3+} in Eu lipo series were measured by the K-shell XRF detection system five times for each sample and the concentrations of Eu^{3+} were estimated using the calibration curve.

Radioluminescence Test with ^{64}Cu Radioisotope

Radioluminescence imaging was demonstrated with liposomes under different conditions (^{64}Cu-Eu lipo, ^{64}Cu-Eu/VBBO lipo, free ^{64}Cu, ^{64}Cu-VBBO lipo, Eu/VBBO lipo, and PBS) by measuring radioluminescence intensity with *in vivo* imaging system (IVIS). For the control group PBS was used in this study. The images were acquired at different wavelength spectra (open, green, and red emission spectrum filters). Quantitative analysis of radioluminescence (RL), Cerenkov luminescence (CL), RL energy transfer (RET), and Cerenkov luminescence energy transfer (CLET) efficiencies were calculated based on the ROI values with IVIS imaging as follows:

CLET=1-CL2/CL1, where CL1 is luminescence intensity of free ^{64}Cu, and CL2 is luminescence intensity of ^{64}Cu-VBBO lipo.

RET=1-RL2/RL1, where RL1 is luminescence intensity of (^{64}Cu-Eu lipo – free ^{64}Cu), and RL2 is luminescence intensity of [^{64}Cu-Eu/VBBO lipo + (free ^{64}Cu - ^{64}Cu-VBBO lipo)], note that RET was adjusted for influence of CLET.

ROS Generation with Radioisotope-Induced Radioluminescence

The degree of ROS generation by radiolabeled liposomes with radioisotope triggered radioluminescence by Eu was determined. In 96-well black microplates 100 μL of free ^{64}Cu, ^{64}Cu-VBBO lipo, and ^{64}Cu-Eu/VBBO lipo were arranged with different ^{64}Cu activities (0, 30, 100, and

200 μCi). Tris-HCl buffer solution (pH 8.0 and 10 mM) was added to activate ROS measurable reagent and 2 μL of SOSG solution (1 μM) was added to each well. The fluorescence intensity of the SOSG reagent at its excitation wavelength (λ_{ex}= 494 nm) was measured in each well. The free ^{64}Cu was used as a control group. An increase degree of ROS generation was calculated to fluorescence intensity ratio between liposomes with and without ^{64}Cu.

***In Vitro* ROS Production**

To confirm the ROS productive cells, Eu/VBBO lipo and ^{64}Cu-Eu/VBBO lipo (^{64}Cu activity: 100 μCi) were treated to the cells and incubated for 24 h. After the incubation, cells were stained with 5 μM of the fluorescent probe (CellROX® Oxidative Stress Reagents, Invitrogen™) for 20 min at 37℃ and the nucleus of the cell was co-stained with 10 μM of Hoechst 33342 (Invitrogen™). The stained cells were washed with DPBS 3 times and fixed with 4% PFA for 30 min, which had also been washed with DPBS 3 times. After the washing steps, the fluorescence levels of the fixed cells were observed by fluorescence optical microscopy (Cell Observer, Carl Zeiss, Oberkochen, Germany).

Preparation of Tumor Model

All animal experiments were performed in accordance with the Institutional Animal Care and Use Committee, Seoul National University Hospital. FaDu tumor bearing Balb/c nude mice were utilized for *in vivo* stable and passive tumor targeted PET imaging. The FaDu cell line (105 cells/20 μL PBS) was injected subcutaneously into the right thigh. The tumor grown mice PET imaging was performed when the implanted tumor reached a required size (mean diameter: 5~10 mm).

***In Vivo* Tumor Targeted PET Imaging of ^{64}Cu Labeled Liposomes**

^{64}Cu labeled VBBO lipo and Eu/VBBO lipo were per-formed *in vivo* imaging with FaDu tumor models. Approximately 200 μL of ^{64}Cu labeled VBBO lipo or Eu/VBBO lipo (~70 μCi

respectively) were injected intravenously into the FaDu tumor bearing mice. The PET scan images were acquired at different time points (0, 2, 12, 24, and 48 h) using PET scanner (GENESYS4). The ROI values were calculated and analyzed for the major organs (heart, liver, spleen, and muscle), including tumor regions with PET images using MIM software for Quantitative analysis. A time activity curve was fitted based on %ID/g at each time point and Tumor targeting efficiency was calculated by comparing the tumor to other organs (heart, muscle, and liver).

***In Vitro* Photodynamic Therapy with ^{64}Cu Labeled Liposomes**

The head and neck cancer FaDu cell line was cultured with Dulbecco's modified Eagle's medium (DMEM), 10% fetal bovine serum (FBS), and 1% penicillin/streptomycin and incubated at 37℃ at 5% CO_2. Once the cell line was covered with about 90% of cell culture in the flask, cells were seeded into 96-well culture plates for cell viability tests (10^4 cells per well) and incubated at 37℃ and 5% CO_2 overnight. After removal of media, ^{64}Cu labeled Eu lipo, VBBO lipo, and Eu/VBBO lipo were added to each well with a different activity (0, 10, 30, and 100 μCi). The control group was cells without any treatment of liposomes. Control and experimental groups were incubated for 24 h. The MTT assay was conducted after all the media and liposomes were re-moved. Cell viability was determined by measuring the absorbance of each well (λ_{abs}= 540 nm).

***In Vivo* Photodynamic Therapy with ^{64}Cu Labeled Liposomes**

^{64}Cu-Eu/VBBO lipo, ^{64}Cu-VBBO lipo, Eu/VBBO lipo, and normal saline were injected intravenously to the FaDu tumor model mice, respectively (Eu^{3+} concentration: 5.3 μmol and VBBO concentration: 6.25 μM). For the radioisotope-induced PDT, each liposome was radiolabeled with ^{64}Cu of 500 μCi activity. Tumor growth follow-ups were conducted for 14 d by acquiring tumor images and measuring the tumor sizes at different time points (0, 2, 8, and 14

days). After the PDT, a tumor in each group was paraffin sectioned and H&E staining was conducted for tumor tissue imaging.

ASSOCIATED CONTENT

Supporting figures from S1 to S16 are included in the Supporting information. The information includes the characterization of nanoparticles, *in vivo* PET analysis, toxicity profile, and excretion analysis. The supporting information are available online and free of charge at.

No potential conflicts of interest relevant to this article exist.

ACKNOWLEDGMENTS

This study was supported by the National Research Foundation of Korea (NRF) (NRF-2017R1D1A1B03035556, NRF-2019M2D2A1A01058210, and 2020R1C1C1009000), the Ministry of Health and Welfare Korea (HI18C0886, and HI19C0339) and Creative-Pioneering Researchers Program through Seoul National University (SNU). We would like to thank Editage (www.editage.co.kr) for English language editing.

REFERENCES

(1) Dolmans, D. E. J. G. J.; Fukumura, D.; Jain, R. K., Photodynamic Therapy for Cancer. *Nat. Rev. Cancer* **2003**, *3*, 380-387.

(2) Castano, A. P.; Mroz, P.; Hamblin, M. R., Photodynamic Therapy and Anti-Tumour Immunity. *Nat. Rev. Cancer* **2006**, *6*, 535-545.

(3) van Straten, D.; Mashayekhi, V.; de Bruijn, H. S.; Oliveira, S.; Robinson, D. J., Oncologic Photodynamic Therapy: Basic Principles, Current Clinical Status and Future Directions. *Cancers* **2017**, *9*, 19.

(4) Shafirstein, G.; Battoo, A.; Harris, K.; Baumann, H.; Gollnick, S. O.; Lindenmann, J.; Nwogu, C. E., Photodynamic Therapy of Non-Small Cell Lung Cancer. Narrative Review and Future Directions. *Ann. Am. Thorac Soc.* **2016**, *13*, 265-275.

(5) Zhou, Z.; Song, J.; Nie, L.; Chen, X., Reactive Oxygen Species Generating Systems Meeting Challenges of Photodynamic Cancer Therapy. *Chem. Soc. Rev.* **2016**, *45*, 6597-6626.

(6) Wang, G. D.; Nguyen, H. T.; Chen, H.; Cox, P. B.; Wang, L.; Nagata, K.; Hao, Z.; Wang, A.; Li, Z.; Xie, J., X-Ray Induced Photodynamic Therapy: A Combination of Radiotherapy and Photodynamic Therapy. *Theranostics* **2016**, *6*, 2295-2305.

(7) Larue, L.; Ben Mihoub, A.; Youssef, Z.; Colombeau, L.; Acherar, S.; Andre, J. C.; Arnoux, P.; Baros, F.; Vermandel, M.; Frochot, C., Using X-Rays in Photodynamic Therapy: An Overview. *Photochem. Photobiol. Sci.* **2018**, *17*, 1612-1650.

(8) Tang, Y.; Hu, J.; Elmenoufy, A. H.; Yang, X., Highly Efficient Fret System Capable of Deep Photodynamic Therapy Established on X-Ray Excited Mesoporous Laf3:Tb Scintillating Nanoparticles. *ACS Appl. Mater. Interfaces* **2015**, *7*, 12261-12269.

(9) Kamkaew, A.; Cheng, L.; Goel, S.; Valdovinos, H. F.; Barnhart, T. E.; Liu, Z.; Cai, W., Cerenkov Radiation Induced Photodynamic Therapy Using Chlorin E6-Loaded Hollow Mesoporous Silica Nanoparticles. *ACS Appl. Mater. Interfaces* **2016**, *8*, 26630-26637.

(10) Ni, D.; Ferreira, C. A.; Barnhart, T. E.; Quach, V.; Yu, B.; Jiang, D.; Wei, W.; Liu, H.; Engle, J. W.; Hu, P.; Cai, W., Magnetic Targeting of Nanotheranostics Enhances Cerenkov Radiation-Induced Photodynamic Therapy. *J. Am. Chem. Soc.* **2018**, *140*, 14971-14979.

(11) Cline, B.; Delahunty, I.; Xie, J., Nanoparticles to Mediate X-Ray-Induced Photodynamic Therapy and Cherenkov Radiation Photodynamic Therapy. *Wiley Interdiscip. Rev. Nanomed. Nanobiotechnol.* **2019**, *11*, e1541.

(12) Pratx, G.; Kapp, D. S., Is Cherenkov Luminescence Bright Enough for Photodynamic Therapy? *Nat. Nanotechnol.* **2018**, *13*, 354-354.

(13) Ciarrocchi, E.; Belcari, N., Cerenkov Luminescence Imaging: Physics Principles and Potential Applications in Biomedical Sciences. *EJNMMI Phys.* **2017**, *4*, 14.

(14) Shrestha, S.; Wu, J.; Sah, B.; Vanasse, A.; Cooper, L. N.; Ma, L.; Li, G.; Zheng, H.; Chen, W.; Antosh, M. P., X-Ray Induced Photodynamic Therapy with Copper-Cysteamine Nanoparticles in Mice Tumors. *Proc. Natl. Acad. Sci. U. S. A.* **2019**, *116*, 16823-16828.

(15) Elmenoufy, A. H.; Tang, Y. a.; Hu, J.; Xu, H.; Yang, X., A Novel Deep Photodynamic Therapy Modality Combined with CT Imaging Established Via X-Ray Stimulated Silica-Modified Lanthanide Scintillating Nanoparticles. *Chem. Commun.* **2015**, *51*, 12247-12250.

(16) Lan, G.; Ni, K.; Xu, R.; Lu, K.; Lin, Z.; Chan, C.; Lin, W., Nanoscale Metal–Organic Layers for Deeply Penetrating X-Ray-Induced Photodynamic Therapy. *Angew. Chem. Int. Ed.* **2017**, *56*, 12102-12106.
(17) Chen, H.; Sun, X.; Wang, G. D.; Nagata, K.; Hao, Z.; Wang, A.; Li, Z.; Xie, J.; Shen, B., Liga5o8:Cr-Based Theranostic Nanoparticles for Imaging-Guided X-Ray Induced Photodynamic Therapy of Deep-Seated Tumors. *Mater. Horiz.* **2017**, *4*, 1092-1101.
(18) Im, H.-J., Excretion and Clearance. In *Radionanomedicine: Combined Nuclear and Nanomedicine*, Lee, D. S., Ed. Springer International Publishing: Cham, 2018; 347-368.
(19) Khlebtsov, N.; Dykman, L., Biodistribution and Toxicity of Engineered Gold Nanoparticles: A Review of *In Vitro* and *In Vivo* Studies. *Chem. Soc. Rev.* **2011**, *40*, 1647-1671.
(20) Yong, K. T.; Law, W. C.; Hu, R.; Ye, L.; Liu, L.; Swihart, M. T.; Prasad, P. N., Nanotoxicity Assessment of Quantum Dots: From Cellular to Primate Studies. *Chem. Soc. Rev.* **2013**, *42*, 1236-1250.
(21) Lee, W.; Im, H. J., Theranostics Based on Liposome: Looking Back and Forward. *Nucl. Med. Mol. Imaging* **2019**, *53*, 242-246.
(22) Mallick, S.; Choi, J. S., Liposomes: Versatile and Biocompatible Nanovesicles for Efficient Biomolecules Delivery. *J. Nanosci. Nanotechnol.* **2014**, *14*, 755-765.
(23) Bunzli, J. C., Benefiting from the Unique Properties of Lanthanide Ions. *Acc. Chem. Res.* **2006**, *39*, 53-61.
(24) Chen, Y.; Guo, W.; Ye, Z.; Wang, G.; Yuan, J., A Europium(III) Chelate as an Efficient Time-Gated Luminescent Probe for Nitric Oxide. *Chem. Commun.* **2011**, *47*, 6266-6268.
(25) Song, B.; Wang, G.; Tan, M.; Yuan, J., A Europium(III) Complex as an Efficient Singlet Oxygen Luminescence Probe. *J. Am. Chem. Soc.* **2006,** *128*, 13442-13450.
(26) Binnemans, K., Lanthanide-Based Luminescent Hybrid Materials. *Chem. Rev.* **2009**, *109*, 4283-4374.
(27) Nishioka, T.; Yuan, J.; Yamamoto, Y.; Sumitomo, K.; Wang, Z.; Hashino, K.; Hosoya, C.; Ikawa, K.; Wang, G.; Matsumoto, K., New Luminescent Europium(III) Chelates for DNA Labeling. *Inorg. Chem.* **2006**, *45*, 4088-4096.
(28) Berezin, M. Y.; Achilefu, S., Fluorescence Lifetime Measurements and Biological Imaging. *Chem. Rev.* **2010**, *110*, 2641-2684.
(29) Selvin, P. R., Principles and Biophysical Applications of Lanthanide-Based Probes. *Annu. Rev. Biophys. Biomol. Struct.* **2002**, *31*, 275-302.
(30) Selvin, P. R.; Hearst, J. E., Luminescence Energy Transfer Using a Terbium Chelate: Improvements on Fluorescence Energy Transfer. *Proc. Natl. Acad. Sci. U. S. A.* **1994**, *91*, 10024-10028.
(31) Hemmila, I.; Laitala, V., Progress in Lanthanides as Luminescent Probes. *J. Fluoresc.* **2005**, *15*, 529-542.
(32) Pandey, P.; Kurchania, R.; Haque, F., Optical Studies of Europium-Doped ZnO Nanoparticles Prepared by Sol–Gel Technique. *J. Adv. Phys.* **2014**, *3*, 104-110.
(33) Ramasamy, S.; Yogamalar, N.; Elanchezhiyan, J.; Joseyphus, J.; Bose, A., Structural and Optical Properties of Europium Doped Yttrium Oxide Nanoparticles for Phosphor Applications. *J. Alloys Compd.* **2010**, *496*, 472-477.
(34) Kumar, A.; Babu, S.; Karakoti, A. S.; Schulte, A.; Seal, S., Luminescence Properties of Europium-Doped Cerium Oxide Nanoparticles: Role of Vacancy and Oxidation States. *Langmuir* **2009**, *25*, 10998-11007.

(35) Chen, H.; Wang, G. D.; Chuang, Y.-J.; Zhen, Z.; Chen, X.; Biddinger, P.; Hao, Z.; Liu, F.; Shen, B.; Pan, Z.; Xie, J., Nanoscintillator-Mediated X-Ray Inducible Photodynamic Therapy for *In Vivo* Cancer Treatment. *Nano Lett.* **2015**, *15*, 2249-2256.
(36) Hsu, C.-C.; Lin, S.-L.; Chang, C. A., Lanthanide-Doped Core–Shell–Shell Nanocomposite for Dual Photodynamic Therapy and Luminescence Imaging by a Single X-Ray Excitation Source. *ACS Appl. Mater. Interfaces* **2018**, *10*, 7859-7870.
(37) Pratt, E. C.; Shaffer, T. M.; Zhang, Q.; Drain, C. M.; Grimm, J., Nanoparticles as Multimodal Photon Transducers of Ionizing Radiation. *Nat. Nanotechnol.* **2018**, *13*, 418-426.
(38) Sun, C.; Pratx, G.; Carpenter, C. M.; Liu, H.; Cheng, Z.; Gambhir, S. S.; Xing, L., Synthesis and Radioluminescence of Pegylated Eu(3+) -Doped Nanophosphors as Bioimaging Probes. *Adv. Mater.* **2011**, *23*, H195-H199.
(39) Hansen, P.-A.; Granerød, C. S.; Prytz, Ø.; Nilsen, O., Controlling Luminescence and Quenching Mechanisms in Subnanometer Multilayer Structure of Europium Titanium Oxide Thin Films. *J. Lumin.* **2019**, *215*, 116618.
(40) Ronda, C., Luminescence Loss Mechanisms. *J. Lumin.* **2009**, *129*, 1824-1826.
(41) Gedanken, A.; Reisfeld, R.; Sominski, L.; Zhong, Z.; Koltypin, Y.; Panczer, G.; Gaft, M.; Minti, H., Time-Dependence of Luminescence of Nanoparticles of Eu2O3 and Tb2O3 Deposited on and Doped in Alumina. *Appl. Phys. Lett.* **2000**, *77*, 945-947.
(42) Larsson, K.; Mezyk, S. P., Employing Luminescence to Determine Eu-DTPA Complex Formation Rate Constants in Lactate and Citrate Media: Experiment and Aggregate-Species Kinetic Modelling. *Solvent Extr. Ion Exch.* **2019**, *37*, 53-64.
(43) Nishioka, T.; Yuan, J.; Yamamoto, Y.; Sumitomo, K.; Wang, Z.; Hashino, K.; Hosoya, C.; Ikawa, K.; Wang, G.; Matsumoto, K., New Luminescent Europium(III) Chelates for DNA Labeling. *Inorg. Chem.* **2006**, *45*, 8460-8460.
(44) Seitz, M.; Moore, E. G.; Ingram, A. J.; Muller, G.; Raymond, K. N., Enantiopure, Octadentate Ligands as Sensitizers for Europium and Terbium Circularly Polarized Luminescence in Aqueous Solution. *J. Am. Chem. Soc.* **2007**, *129*, 15468-15470.
(45) Heyduk, T., Luminescence Resonance Energy Transfer Analysis of RNA Polymerase Complexes. *Methods* **2001**, *25*, 44-53.
(46) Kokko, T. Lanthanide Chelates as Donors in Fluorescence Resonance Energy Transfer: Exciting Prospects for Bioaffinity Assay Detection. University of Turku, 2009.
(47) Hu, D.; Sheng, Z.; Zhu, M.; Wang, X.; Yan, F.; Liu, C.; Song, L.; Qian, M.; Liu, X.; Zheng, H., Förster Resonance Energy Transfer-Based Dual-Modal Theranostic Nanoprobe for *In Situ* Visualization of Cancer Photothermal Therapy. *Theranostics* **2018**, *8*, 410-422.
(48) Jung, S.; Kim, T.; Lee, W.; Kim, H.; Kim, H. S.; Im, H. J.; Ye, S. J., Dynamic *In Vivo* X-Ray Fluorescence Imaging of Gold in Living Mice Exposed to Gold Nanoparticles. *IEEE Trans. Med. Imaging* **2019**, *39*, 526-533.
(49) Jones, G.; Bradshaw, D., Resonance Energy Transfer: From Fundamental Theory to Recent Applications. *Front. Phys.* **2019**, *7*.

(50) Niccoli Asabella, A.; Cascini, G. L.; Altini, C.; Paparella, D.; Notaristefano, A.; Rubini, G., The Copper Radioisotopes: A Systematic Review with Special Interest to 64Cu. *Biomed. Res. Int.* **2014**, *2014*, 786463-786463.
(51) Love, C.; Din, A. S.; Tomas, M. B.; Kalapparambath, T. P.; Palestro, C. J., Radionuclide Bone Imaging: An Illustrative Review. *Radiographics* **2003**, *23*, 341-358.
(52) Taylor, A. T., Radionuclides in Nephrourology, Part 1: Radiopharmaceuticals, Quality Control, and Quantitative Indices. *J. Nucl. Med.* **2014**, *55*, 608-615.

(53) Baggish, A. L.; Boucher, C. A., Radiopharmaceutical Agents for Myocardial Perfusion Imaging. *Circulation* **2008**, *118*, 1668-1674.
(54) Kotagiri, N.; Cooper, M. L.; Rettig, M.; Egbulefu, C.; Prior, J.; Cui, G.; Karmakar, P.; Zhou, M.; Yang, X.; Sudlow, G.; Marsala, L.; Chanswangphuwana, C.; Lu, L.; Habimana-Griffin, L.; Shokeen, M.; Xu, X.; Weilbaecher, K.; Tomasson, M.; Lanza, G.; DiPersio, J. F.*, et al.*, Radionuclides Transform Chemotherapeutics into Phototherapeutics for Precise Treatment of Disseminated Cancer. *Nat. Commun.* **2018**, *9*, 275.
(55) Unger, E.; Cardenas, D.; Zerella, A.; Fajardo, L. L.; Tilcock, C., Biodistribution and Clearance of Liposomal Gadolinium-DTPA. *Invest. Radiol.* **1990**, *25*, 638-644.
(56) Chatterjee, D. K.; Fong, L. S.; Zhang, Y., Nanoparticles in Photodynamic Therapy: An Emerging Paradigm. *Adv. Drug. Deliv. Rev.* **2008**, *60*, 1627-1637.
(57) Jin, C. S.; Zheng, G., Liposomal Nanostructures for Photosensitizer Delivery. *Lasers Surg. Med.* **2011**, *43*, 734-748.
(58) Wilhelm, S.; Tavares, A. J.; Dai, Q.; Ohta, S.; Audet, J.; Dvorak, H. F.; Chan, W. C. W., Analysis of Nanoparticle Delivery to Tumours. *Nat. Rev. Mater.* **2016**, *1*, 16014.
(59) de Souza, A. L. R.; LaRochelle, E.; Marra, K.; Gunn, J.; Davis, S. C.; Samkoe, K. S.; Chapman, M. S.; Maytin, E. V.; Hasan, T.; Pogue, B. W., Assessing Daylight & Low-Dose Rate Photodynamic Therapy Efficacy, Using Biomarkers of Photophysical, Biochemical and Biological Damage Metrics *In Situ*. *Photodiagn. Photodyn.* **2017**, *20*, 227-233.
(60) Conti, M.; Eriksson, L., Physics of Pure and Non-Pure Positron Emitters for PET: A Review and a Discussion. *EJNMMI Phys.* **2016**, *3*, 8.
(61) Kotagiri, N.; Sudlow, G. P.; Akers, W. J.; Achilefu, S., Breaking the Depth Dependency of Phototherapy with Cerenkov Radiation and Low-Radiance-Responsive Nanophotosensitizers. *Nat. Nanotechnol.* **2015**, *10*, 370-379.
(62) Strosberg, J.; El-Haddad, G.; Wolin, E.; Hendifar, A.; Yao, J.; Chasen, B.; Mittra, E.; Kunz, P. L.; Kulke, M. H.; Jacene, H.; Bushnell, D.; O'Dorisio, T. M.; Baum, R. P.; Kulkarni, H. R.; Caplin, M.; Lebtahi, R.; Hobday, T.; Delpassand, E.; Van Cutsem, E.; Benson, A.*, et al.*, Phase 3 Trial of 177lu-Dotatate for Midgut Neuroendocrine Tumors. *N. Engl. J. Med.* **2017**, *376*, 125-135.
(63) von Eyben, F. E.; Roviello, G.; Kiljunen, T.; Uprimny, C.; Virgolini, I.; Kairemo, K.; Joensuu, T., Third-Line Treatment and (177)Lu-PSMA Radioligand Therapy of Metastatic Castration-Resistant Prostate Cancer: A Systematic Review. *Eur. J. Nucl. Med. Mol. Imaging* **2018**, *45*, 496-508.
(64) Hofman, M. S.; Violet, J.; Hicks, R. J.; Ferdinandus, J.; Thang, S. P.; Akhurst, T.; Iravani, A.; Kong, G.; Ravi Kumar, A.; Murphy, D. G.; Eu, P.; Jackson, P.; Scalzo, M.; Williams, S. G.; Sandhu, S., [(177)Lu]-PSMA-617 Radionuclide Treatment in Patients with Metastatic Castration-Resistant Prostate Cancer (Lupsma Trial): A Single-Centre, Single-Arm, Phase 2 Study. *Lancet Oncol.* **2018**, *19*, 825-833.
(65) Haley, T. J.; Komesu, N.; Colvin, G.; Koste, L.; Upham, H. C., Pharmacology and Toxicology of Europium Chloride. *J. Pharm. Sci.* **1965**, *54*, 643-645.
(66) Ogawa, Y.; Suzuki, S.; Naito, K.; Saito, M.; Kamata, E.; Hirose, A.; Ono, A.; Kaneko, T.; Chiba, M.; Inaba, Y., Toxicity Study of Europium Chloride in Rats. *J. Environ. Pathol. Toxicol. Oncol.* **1995**, *14*, 1-9.
(67) Rim, K. T.; Koo, K. H.; Park, J. S., Toxicological Evaluations of Rare Earths and Their Health Impacts to Workers: A Literature Review. *Saf. Health Work* **2013**, *4*, 12-26.

(68) Weinmann, H. J.; Brasch, R. C.; Press, W. R.; Wesbey, G. E., Characteristics of Gadolinium-DTPA Complex: A Potential NMR Contrast Agent. *AJR, Am. J. Roentgenol.* **1984**, *142*, 619-624.

(69) Wagner, A.; Vorauer-Uhl, K., Liposome Technology for Industrial Purposes. *J. Drug Deliv.* **2011**, *2011,* 591325.